JVI Journals.ASM.org

HIV-1 Uncoating Is Facilitated by Dynein and Kinesin 1

Zana Lukic,[a] Adarsh Dharan,[b] Thomas Fricke,[c] Felipe Diaz-Griffero,[c] Edward M. Campbell[a,b]

Integrative Cell Biology Program, Stritch School of Medicine, Loyola University Chicago, Maywood, Illinois, USA[a]; Department of Microbiology and Immunology, Stritch School of Medicine, Loyola University Chicago, Maywood, Illinois, USA[b]; Department of Microbiology and Immunology, Albert Einstein College of Medicine, Bronx, New York, USA[c]

ABSTRACT

Following entry into the target cell, human immunodeficiency virus type 1 (HIV-1) must reverse transcribe its RNA genome to DNA and traffic to the nuclear envelope, where the viral genome is translocated into the nucleus for subsequent integration into the host cell chromosome. During this time, the viral core, which houses the genome, undergoes a poorly understood process of disassembly, known as uncoating. Collectively, many studies suggest that uncoating is tightly regulated to allow nuclear import of the genome while minimizing the exposure of the newly synthesized DNA to cytosolic DNA sensors. However, whether host cellular proteins facilitate this process remains poorly understood. Here we report that intact microtubules facilitate HIV-1 uncoating in target cells. Disruption of microtubules with nocodazole substantially delays HIV-1 uncoating, as revealed with three different assay systems. This defect in uncoating did not correlate with defective reverse transcription at early times postinfection, demonstrating that microtubule-facilitated uncoating is distinct from the previously reported role of viral reverse transcription in the uncoating process. We also find that pharmacological or small interfering RNA (siRNA)-mediated inhibition of cytoplasmic dynein or the kinesin 1 heavy chain KIF5B delays uncoating, providing detailed insight into how microtubules facilitate the uncoating process. These studies reveal a previously unappreciated role for microtubules and microtubule motor function in HIV-1 uncoating, establishing a functional link between viral trafficking and uncoating. Targeted disruption of the capsid motor interaction may reveal novel mechanisms of inhibition of viral infection or provide opportunities to activate cytoplasmic antiviral responses directed against capsid or viral DNA.

IMPORTANCE

During HIV-1 infection, fusion of viral and target cell membranes dispenses the viral ribonucleoprotein complex into the cytoplasm of target cells. During this time, the virus must reverse transcribe its RNA genome, traffic from the location of fusion to the nuclear membrane, and undergo the process of uncoating, whereby the viral capsid core disassembles to allow the subsequent nuclear import of the viral genome. Numerous cellular restriction factors target the viral capsid, suggesting that perturbation of the uncoating process represents an excellent antiviral target. However, this uncoating process, and the cellular factors that facilitate uncoating, remains poorly understood. The main observation of this study is that normal uncoating requires intact microtubules and is facilitated by dynein and kinesin motors. Targeting these factors may either directly inhibit infection or delay it enough to trigger mediators of intrinsic immunity that recognize cytoplasmic capsid or DNA and subsequently induce an antiviral state in these cells.

Following the fusion of viral and host target cell membranes, human immunodeficiency virus type 1 (HIV-1) core is released into the target cell cytoplasm. Following release, critical early events of the viral life cycle take place in the cytoplasm. Inside the viral core, reverse transcriptase begins converting the viral RNA genome into DNA. Additionally, the viral ribonucleoprotein complex must traffic from the point of fusion to the nuclear envelope in order to allow the nuclear import of the genome for subsequent integration. During this time, the viral core undergoes uncoating, the process by which the viral capsid (CA) disassembles to allow the genome housed within the core to be imported into the nucleus.

Of these cytoplasmic events, reverse transcription (RT) is the best-understood process (1). A detailed understanding of reverse transcriptase, the viral polymerase that converts the viral RNA genome into DNA, has led to the development of numerous inhibitors that are currently used to prevent viral replication in HIV-1-positive individuals. Kinetically, reverse transcription is thought to initiate quickly following entry into a permissive target cell, with the accumulation of late reverse transcripts peaking 6 to 12 h after infection (2).

Unlike reverse transcription, uncoating remains one of the most poorly understood steps in the viral life cycle. Specifically, it is not clear how the mature capsid core disassembles to allow the nuclear translocation of the lentiviral genome. Biochemically, HIV-1 cores are less stable than the cores of simple retroviruses, such as murine leukemia virus (MLV) (3, 4), which require the breakdown of the nuclear envelope during mitosis to access cellular DNA. Biochemical isolation and immunofluorescent staining of HIV-1 reverse transcription complexes (RTCs) have demonstrated that there is a substantial loss in the CA content (3, 5, 6). Other studies have exploited the ability of the owl monkey restric-

Received 30 July 2014 **Accepted** 8 September 2014
Published ahead of print 17 September 2014
Editor: S. R. Ross
Address correspondence to Edward M. Campbell, ecampbell@luc.edu.
Z.L. and A.D. contributed equally to this article.
Supplemental material for this article may be found at http://dx.doi.org/10.1128/JVI.02219-14.

doi:10.1128/JVI.02219-14

tion factor TRIM-Cyp, which targets CA on the incoming virion, to define the period during which the core remains intact following infection. This assay revealed that virions become insensitive to TRIM-Cyp restriction rapidly (7, 8), with an uncoating "half-life" of 39 min following fusion (7). Collectively, these studies suggest that some form of uncoating occurs rapidly following the entry of the viral core into the target cell cytoplasm. However, it is also clear that the nuclear import of the viral genome is mediated by CA (9–12). These studies demonstrate that some CA protein must remain associated with the viral RTC during trafficking to the nuclear pore. HIV-1 trafficking to the nuclear pore is thought to involve microtubule-mediated transport. McDonald et al. have demonstrated that the trafficking of green fluorescent protein (GFP)-Vpr-labeled HIV-1 toward the microtubule-organizing center (MTOC) is mediated by dynein-dependent transport (6). Recently, another study has reported that EB1, a protein that recruits plus-end trafficking proteins (+TIPs) to stabilize microtubules, facilitates HIV-1 infection (13). These studies support a role for microtubules in HIV-1 trafficking and infection.

These early events of infection are not temporally distinct. Rather, they are likely to be going on simultaneously and to exhibit some degree of interdependency. For example, Hulme et al. have demonstrated that capsid uncoating is stimulated by viral reverse transcription within the capsid core (7). However, no connection has been observed between uncoating and the trafficking of the viral core. Here we report that core uncoating requires intact microtubules, since disruption of microtubules with nocodazole inhibits uncoating. We extend this observation by determining that uncoating is driven by the microtubule motor proteins dynein and kinesin 1. These observations establish a critical connection between trafficking and uncoating, revealing a new mechanism by which HIV-1 coopts the cellular machinery to facilitate its life cycle.

MATERIALS AND METHODS

Cell lines, tissue culture, and drugs. Owl monkey kidney (OMK) cells (kindly provided by Theodora Hatziioannou), as well as CF2Th, HeLa, and 293T cells, were cultured in Dulbecco's modified Eagle medium (DMEM) (Cellgro) supplemented with 10% fetal bovine serum (FBS), 1,000 U/ml penicillin, 1,000 U/ml streptomycin, and 10 μg/ml ciprofloxacin hydrochloride. Nocodazole (Noc) (Cayman Chemical) was used at a final concentration of 10 μM; cyclosporine (CsA; Sigma-Aldrich) was used at a final concentration of 2.5 μM; and ciliobrevin D (CilioD) (Millipore) was used at a final concentration of 100 μM in medium containing 1% FBS rather than 10% FBS due to the serum requirement for this drug to be functional.

Generation of stable cell lines. Lentivirus for transduction was produced by transfection of 293T cells with 1 μg pLVX-HA-TRIMCyp, 1 μg ΔNRF (nuclear respiratory factor) packaging construct, and 1 μg vesicular stomatitis virus glycoprotein (VSV-G) by using polyethylenimine (PEI; molecular weight, 25,000; Polysciences) in a 60-mm dish. Viruses were harvested 48 h after transfection, filtered through a 0.45-μm filter (Millipore), and used to transduce HeLa cells. Forty-eight hours after transduction, cells were selected in DMEM containing 5 μg/ml puromycin (Sigma-Aldrich). Expression of hemagglutinin (HA)-TRIM-Cyp was confirmed by Western blotting, and restriction capability was confirmed by infection with HIV-1.

Western blotting. Whole-cell lysates were prepared by lysing cells with NP-40 lysis buffer (100 mM Tris [pH 8.0], 1% NP-40, 150 mM NaCl) containing protease inhibitor cocktail (Roche) for 10 min on ice. Following the incubation on ice, 2× Laemmli sample buffer was added to the lysed cells, which were incubated at 100°C for 10 min. Samples were loaded onto a 10% polyacrylamide gel for sodium dodecyl sulfate-polyacrylamide gel electrophoresis (SDS-PAGE). After separation, the proteins were transferred to nitrocellulose membranes (Bio-Rad) and were detected by incubation with horseradish peroxidase (HRP)-conjugated anti-HA (Thermo Scientific), anti-β-actin (University of Iowa Hybridoma Bank), and antibodies to dynein heavy chain (DYNC1H1) (Abcam), and kinesin 1 heavy chain (KHC) (Abcam). Antibody complexes were detected using SuperSignal West Femto chemiluminescent substrate (Thermo Scientific). Chemiluminescence was detected using the UVP EC3 imaging system (UVP LLC).

Virus production and synchronized infection. To generate pseudotyped HIV-1, 293T cells seeded in a 25-cm dish at 60% confluence were transfected with 7.85 μg pCMV-VSVg or pCMB-AMLV and 14.60 μg of R7ΔEnvGFP by using PEI. Viruses were harvested 48 h after transfection, spun for 5 min at 1,200 rpm, and filtered through a 0.45-μm filter (Millipore). Synchronized infections were performed as described previously (14). Specifically, cells were spinoculated at 13°C for 2 h at 1,200 × *g*, after which time all the virus was removed and was replaced with 37°C medium containing the relevant drugs, as described for each experiment. Virus stocks were titrated on cells used in subsequent experiments, and the percentage of green fluorescent protein (GFP)-positive cells was determined using a BD FACSCanto II flow cytometer (BD Biosciences).

siRNA transfection and knockdown. All small interfering RNA (siRNA) sequences used were obtained from previously published works and have been shown to target the protein of interest. siRNA duplexes targeting the dynein heavy chain (DYNC1H1) (15, 16) or kinesin 1 heavy chain (KIF5B) (Fisher Scientific) (17) were synthesized. An siRNA targeting the luciferase gene from Fisher Scientific was used as a control in all siRNA experiments. The siRNAs were transfected into HeLa cells plated on 6-well dishes by using the Lipofectamine 2000 reagent (Thermo Fisher). A second transfection was performed 24 h later. After 72 h of the first transfection, cells were collected and were plated on 24-well plates, followed by synchronized infection a day later. Cells were collected during infection for Western blotting to monitor the knockdown efficiency of the siRNA.

CsA withdrawal assays. OMK cells (kindly provided by Theodora Hatziioannou) and HeLa cells expressing HA-TRIM-Cyp were plated in 24-well plates. Cells were spinoculated with a GFP reporter virus in the presence of CsA with either dimethyl sulfoxide (DMSO), nocodazole, or ciliobrevin D for 2 h at 13°C and 1,200 × *g*. Following spinoculation, the medium was aspirated and was replaced with warm medium containing drugs, and cells were incubated at 37°C. Washout of CsA continued throughout the time course. After 2 or 4 h, nocodazole, paclitaxel, and ciliobrevin D were removed by washing the cells generously with phosphate-buffered saline (PBS) and adding back warm medium containing CsA to be washed out at subsequent time points. At time points before 2 h, CsA was removed and was replaced with Noc or DMSO only, which was washed out 2 h following infection. CsA washout was performed until 4 h postspinoculation, since it is known from previous studies (18, 19) that the vast majority of the infectious inoculum will have escaped TRIM-Cyp restriction by 4 h. Controls included nocodazole, and ciliobrevin D without CsA, as well as continuous DMSO treatment. Two days following the time course, cells were harvested and were fixed in 1× PBS (Cellgro) containing 2% formaldehyde (Polysciences). The percentage of GFP-positive cells was determined using a BD FACSCanto II flow cytometer (BD Biosciences).

BlaM-Vpr fusion assay. Cells were infected with VSVg-R7ΔEnvGFP by spinoculation in presence or absence of drugs. Following spinoculation, the medium was removed and was replaced with warm medium containing the relevant drugs. Cells were incubated at 37°C for 3 h, followed by CCF2-AM (Invitrogen) loading of the cells according to the manufacturer's protocol. The reaction was allowed to proceed overnight at room temperature, and the cells were collected and analyzed by flow cytometry for CCF2-AM cleavage.

Fluorescent microscopy. Z-stack images were collected using identical acquisition parameters with a DeltaVision wide-field fluorescence mi-

croscope (Applied Precision, GE) equipped with a digital camera (CoolSNAP HQ; Photometrics), using a 1.4-numerical-aperture 100× objective lens. Excitation light was generated with an InsightSSI solid-state illumination module (Applied Precision, GE), and images were deconvolved with softWoRx deconvolution software (Applied Precision, GE). Following deconvolution, images were quantified by Imaris software (Bitplane) using the Surfaces feature and generating surfaces around GFP-Vpr puncta. The maximum fluorescence intensities of the S15-mCherry and Cy5 channels within each surface were calculated for each deconvolved image in the data set and were compiled using Prism, version 6 (GraphPad).

***In situ* uncoating assay.** To generate fluorescently labeled HIV-1, 293T cells seeded in a 25-cm dish at 60% confluence were transfected with 8.45 μg S15-mCherry, 2.8 μg GFP-Vpr, 6.75 μg R7ΔEnvGFP, and 4.5 μg pCMV-VSVg using PEI. S15-mCherry is a fluorescent fusion protein that contains the 15 N-terminal amino acids of the cellular Src protein. This 15-amino-acid sequence contains a myristoylation sequence that is sufficient to cause membrane association and incorporation of S15-mCherry into the virion. Following fusion, the S15-mCherry-labeled viral membrane is lost, which allows for effective distinction between virions that have been nonproductively endocytosed by the target cells (S15-mCherry positive, GPF-Vpr positive) and those that have productively fused into the cytoplasm (S15-mCherry negative, GFP-Vpr positive). Two days following the transfections, the virus was collected, centrifuged at 2,000 rpm for 5 min, and filtered through a 0.45-μm filter (Millipore). Harvested viruses were spinoculated on coverslips and were stained for p24 using anti-p24 monoclonal antibody (MAb) AG3.0 (obtained from Jonathan Allan [20] through the NIH AIDS Reagent Program, Division of AIDS, NIAID, NIH) in blocking solution (10% normal donkey serum [Jackson ImmunoResearch Laboratories], 0.1% saponin, 0.01% NaN_3 in PBS) for 1 h at room temperature, followed by a secondary antibody conjugated to Cy5 (Jackson ImmunoResearch Laboratories) for 30 min at room temperature in the same blocking solution. Background levels after antibody treatment were assessed using a secondary-antibody-only control or an isotype control against mouse IgG1 at a concentration of 1 μg/ml (Thermo Fisher). Labeling efficiency was assessed by determining the percentage of virions in a field that were positive for S15-mCherry, GFP-Vpr, and p24. For infections, OMK and HeLa cells were seeded on fibronectin-treated coverslips, and synchronized infection was carried out in the presence or absence of the drugs of interest. Following spinoculation, the medium was aspirated and was replaced with warm medium containing drugs, and cells were incubated at 37°C. At various time points postinfection, coverslips were fixed with 3.75% formaldehyde in 0.159 M piperazine-*N*,*N*′-bis(2-ethanesulfonic acid) (PIPES) buffer (pH 6.8) for 5 min and were washed with 1× PBS. Coverslips were stained with anti-p24 MAb AG3.0 as described above and were mounted on glass slides with Gel Mount (Biomedia).

Fate-of-capsid assay. The fate-of-capsid assay was performed as described previously (21, 22). HIV-1 virus-like particles (VLPs) were produced by calcium phosphate cotransfection of plasmids containing the genes encoding HIV-1 Gag-Pol, VSV-G envelope, and Rev protein at a ratio of 15:3:1 by weight. Stably transduced Cf2Th cells (1.5×10^6) expressing the indicated proteins were seeded in 80-cm^2 flasks. The following day, the cells were incubated with 5 to 10 ml of HIV-1 (approximately 2.5×10^5 to 5.0×10^5 reverse transcriptase units) at 4°C for 30 min to allow viral attachment to the cells. The cells were then shifted to 37°C, treated with nocodazole for 4 h, and collected at 16 h postinfection. Cells were washed three times with ice-cold PBS and were detached by treatment with 1.0 ml of pronase (7.0 mg/ml in DMEM) for 5 min at 25°C. The cells were then washed three times with PBS. The cells were resuspended in 2.5 ml hypotonic lysis buffer (10 mM Tris-HCl [pH 8.0], 10 mM KCl, 1 mM EDTA, and one Complete protease inhibitor tablet) and were incubated on ice for 15 min. The cells were lysed using 15 strokes in a 7.0-ml Dounce homogenizer with pestle B. Cellular debris was cleared by centrifugation for 3 min at 3,000 rpm. To allow assessment of the input for HIV-1 p24, 100 μl of the cleared lysate was collected, diluted to 1× in SDS sample buffer, and analyzed by Western blotting. Then 2.0 ml of the cleared lysate was layered onto a 50% (wt/vol) sucrose cushion in 1× PBS and was centrifuged at 125,000 × *g* for 2 h at 4°C in a Beckman SW41 rotor. Following centrifugation, 100 μl of the topmost portion of the supernatant was collected and diluted to 1× in SDS sample buffer; this sample is referred to as the soluble fraction. The pellet was resuspended in 50 μl 1× SDS sample buffer and is referred to as the particulate capsid. All samples were then subjected to SDS-PAGE and Western blotting. The HIV-1 p24 proteins were detected using a mouse anti-p24 antibody (ImmunoDiagnostics).

Real-time PCR. In conjunction with CsA washout assays, samples were collected for real-time PCR (RT-PCR) at various hours after infection with or without drugs. Genomic DNA was extracted from cells by following the DNeasy blood and tissue kit protocol (Qiagen). The concentration of genomic DNA was determined using a NanoDrop 1000 instrument (Thermo Scientific), and genomic DNA was digested with DpnI (New England BioLabs). Real-time PCR was performed as described previously with primers for late reverse transcription, circles containing two long terminal repeats (2-LTR circles), and β-actin (2, 23).

Statistical analysis. Statistical significance was assessed using the Student *t* test or a multiple-comparison test whenever two groups were compared. Data are represented as means ± standard errors of the means (SEM) or standard deviations (SD) depending on the graph. When more than two groups were compared, one-way analysis of variance (ANOVA) was used. Calculations were performed in GraphPad Prism software (GraphPad Software, Inc.).

RESULTS

Microtubule disruption delays the uncoating kinetics of HIV-1. To test the hypothesis that microtubule trafficking facilitates HIV-1 uncoating, we utilized the cyclosporine (CsA) withdrawal assay, which was employed previously to assess the uncoating kinetics of the HIV-1 capsid during infection (7, 8, 24). This assay exploits the TRIM-Cyp restriction factor from owl monkeys, which utilizes a C-terminal cyclophilin A (CypA) domain to bind HIV-1 cores, leading to potent inhibition of infection (25). This C-terminal CypA domain is also sensitive to the immunosuppressive drug CsA, such that infection of cells expressing TRIM-Cyp in the presence of CsA completely relieves HIV-1 restriction (25). Moreover, by withdrawal of CsA from cells at specific intervals following a synchronized infection, the rate of uncoating can be measured as the percentage of the viral inoculum that has become insensitive to TRIM-Cyp restriction at the time of withdrawal (reviewed in reference 24). We observed that, as reported previously (7), the vast majority of the viral inoculum had become insensitive to TRIM-Cyp restriction following CsA withdrawal 4 h after a synchronized infection (data not shown). Therefore, we infected owl monkey kidney (OMK) cells with VSV-G-pseudotyped HIV-1 in the presence or absence of 10 μM nocadozole (Noc) for 2 h and monitored uncoating by using CsA withdrawal after infection. The 2-h treatment criterion was based on the half-life of uncoating as described previously (7) and also on the observation that Noc treatment of this duration at this concentration exhibited no appreciable toxicity to cells. Cells treated with Noc exhibited less uncoating during the 2-h treatment than DMSO-treated cells. Notably, when Noc was withdrawn, the viral inoculum in these cells rapidly became insensitive to CsA withdrawal, thus eliminating the delay in uncoating in these cells (Fig. 1A and B). To ensure that HIV-1 infection and TRIM-Cyp restriction were not perturbed by Noc treatment, we also performed parallel infections in which CsA was present overnight or was entirely

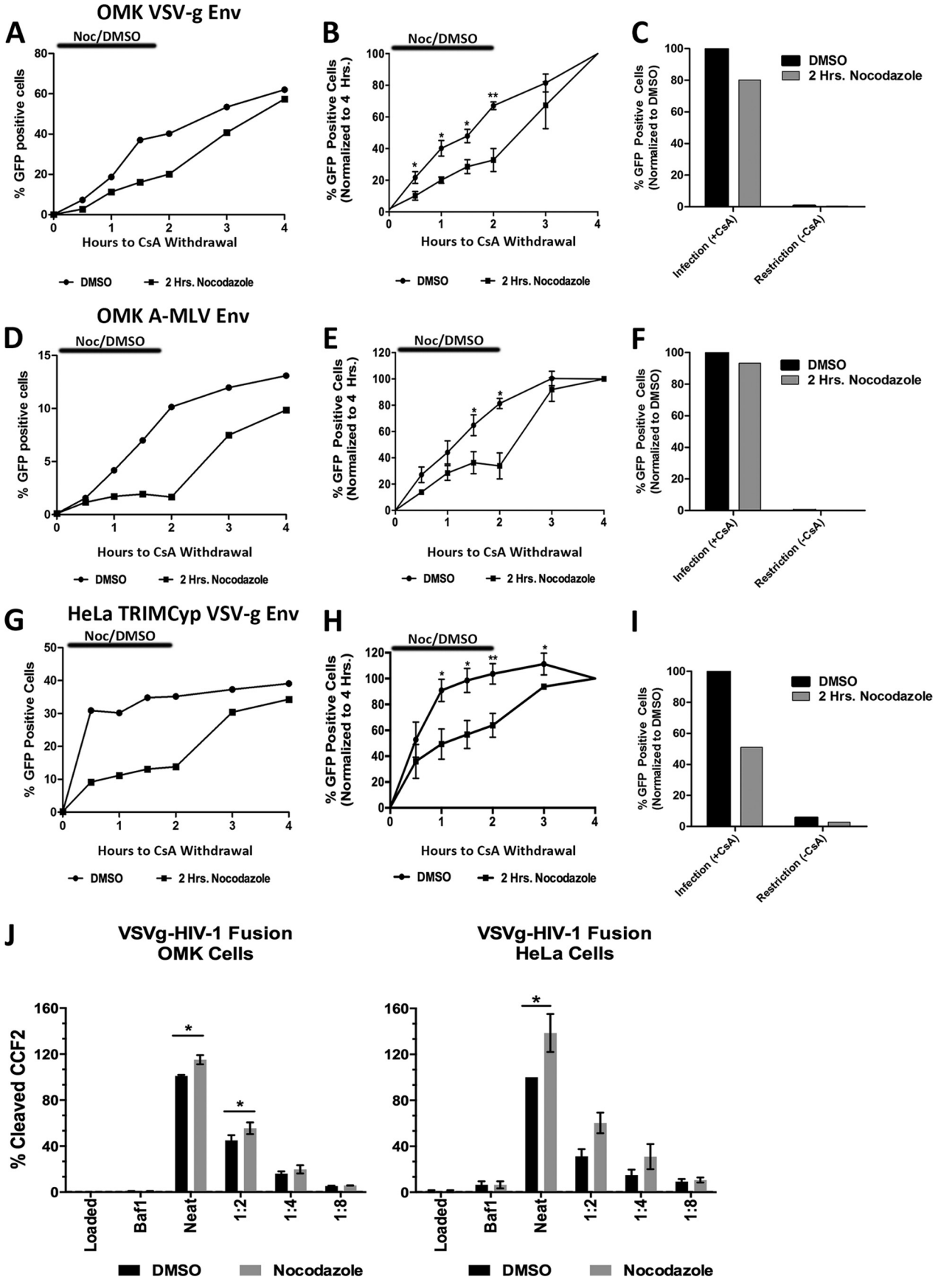
OMK VSV-g Env
A
Noc/DMSO
% GFP positive cells
Hours to CsA Withdrawal
DMSO
2 Hrs. Nocodazole
B
Noc/DMSO
% GFP Positive Cells (Normalized to 4 Hrs.)
Hours to CsA Withdrawal
DMSO
2 Hrs. Nocodazole
C
% GFP Positive Cells (Normalized to DMSO)
DMSO
2 Hrs. Nocodazole
Infection (+CsA)
Restriction (-CsA)
OMK A-MLV Env
D
Noc/DMSO
% GFP positive cells
Hours to CsA Withdrawal
DMSO
2 Hrs. Nocodazole
E
Noc/DMSO
% GFP Positive Cells (Normalized to 4 Hrs.)
Hours to CsA Withdrawal
DMSO
2 Hrs. Nocodazole
F
% GFP Positive Cells (Normalized to DMSO)
DMSO
2 Hrs. Nocodazole
Infection (+CsA)
Restriction (-CsA)
HeLa TRIMCyp VSV-g Env
G
Noc/DMSO
% GFP Positive Cells
Hours to CsA Withdrawal
DMSO
2 Hrs. Nocodazole
H
Noc/DMSO
% GFP Positive Cells (Normalized to 4 Hrs.)
Hours to CsA Withdrawal
DMSO
2 Hrs. Nocodazole
I
% GFP Positive Cells (Normalized to DMSO)
DMSO
2 Hrs. Nocodazole
Infection (+CsA)
Restriction (-CsA)
J
VSVg-HIV-1 Fusion OMK Cells
VSVg-HIV-1 Fusion HeLa Cells
% Cleaved CCF2
Loaded
Baf1
Neat
1:2
1:4
1:8
DMSO
Nocodazole

absent from the culture medium of the infected cells. In the presence of CsA, infection was only modestly affected by Noc treatment (Fig. 1C), in agreement with a previous report that transient Noc treatment does not inhibit HIV-1 infection (26). Transient Noc treatment did not disrupt the ability of TRIM-Cyp to restrict HIV-1 infection (Fig. 1C). This effect was not due to a defect in fusion mediated by Noc, since the level of fusion of VSV-G-pseudotyped HIV-1 loaded with Vpr–β-lactamase (27) was not reduced by Noc treatment. Instead, we consistently observed a small but statistically significant increase in the level of fusion in the presence of Noc (Fig. 1J). However, to ensure that perturbed vesicular trafficking, and thus VSV-G-mediated fusion, was not responsible for the delay in uncoating observed with Noc treatment, we also performed the same experiment using HIV-1 pseudotyped with the pH-independent amphotropic MLV envelope (A-MLV Env) (Fig. 1D and E). Again, cells treated with Noc exhibited delayed uncoating relative to that of DMSO-treated cells, but cells infected with A-MLV-pseudotyped HIV-1 recovered even more rapidly following Noc withdrawal than cells infected with VSV-G-pseudotyped virus, typically exhibiting an even more marked delay during Noc treatment and more rapid uncoating after Noc withdrawal. As was observed for VSV-G-pseudotyped virus, Noc treatment did not perturb HIV-1 infection or TRIM-Cyp restriction in these cells (Fig. 1F). We also performed similar experiments using HeLa cells stably expressing OMK TRIM-Cyp. As was observed in OMK cells, Noc treatment delayed HIV-1 uncoating, increasing the sensitivity of the viral inoculum to TRIM-Cyp at early time points (Fig. 1G and H). In HeLa cells, although infectivity was not substantially affected when CsA was withdrawn at 4 h (Fig. 1G), 2 h of Noc treatment followed by overnight incubation with CsA did result in a modest reduction of infectivity (Fig. 1I).

Rapid recovery of microtubules following Noc withdrawal. One interpretation of the rapid restoration of uncoating observed following Noc withdrawal in these experiments is that microtubules rapidly re-form following Noc withdrawal, allowing uncoating to recover more quickly than in DMSO-treated cells. We therefore examined the state of microtubules in these cells after a 2-h Noc treatment and 1 h after Noc withdrawal (Fig. 2). We observed that after a 2-h Noc treatment, the microtubule network in OMK cells was disrupted. The majority of these cells exhibited no intact microtubules, while ~25% of these cells retained some fragmented microtubules (Fig. 2). HeLa cells exhibited a slightly different response to 2 h of Noc treatment: the majority of these cells contained fragmented microtubules, while a smaller population had completely depolymerized microtubules (Fig. 2). However, in both cell types, the microtubule network recovered rapidly following Noc withdrawal, such that intact microtubules were present 15 min after Noc withdrawal (Fig. 2). By 1 h after Noc withdrawal, visibly normal microtubule networks had re-formed in both cell lines. Collectively, these data suggest that disruption of the microtubule network with Noc inhibits HIV-1 core uncoating, since the viral inoculum remained sensitive to TRIM-Cyp restriction longer in Noc-treated cells than in control-treated cells. Following Noc withdrawal, the microtubule network quickly reforms, and this correlates with a rapid restoration of uncoating in Noc-treated cells, consistent with the hypothesis that the microtubule network facilitates the uncoating of the HIV-1 capsid core.

Effect of microtubule disruption on uncoating kinetics as determined by an *in situ* fluorescence microscopy assay. To confirm that Noc treatment affects HIV-1 uncoating, we analyzed the uncoating states of individual virions following a synchronized infection. To do this, we utilized HIV-1 virions labeled with GFP-Vpr, which allows visualization of the viral ribonucleoprotein complex (6), and S15-mCherry, which allows assessment of the fusion statuses of individual virions (28). This label allows unfused virions that have not productively entered the cell via fusion, and thus remain within the vesicular compartment, to be removed from our analysis. To measure the amounts of p24 CA associated with individual virions, we stained them with a monoclonal antibody to p24 and measured the p24-associated fluorescence of individual GFP-Vpr-positive viral particles using wide-field deconvolution microscopy (Fig. 3A). Importantly, the field uniformity and sensitivity of detection of wide-field deconvolution systems such as the one we utilize here make it ideally suited for the quantitative interrogation of CA signals associated with individual viral complexes (29, 30).

This established a system by which we could measure the amount of p24 associated with individual cytoplasmic virions that have productively entered the cell. Background staining in this system was assessed using a secondary antibody only or an isotype control and showed the anti-p24 antibody AG3.0 to be highly selective in detecting the viral capsid present in individual GFP-Vpr-positive particles (Fig. 3B). We also utilized software-assisted identification of GFP-Vpr viral complexes to determine the maximal S15-mCherry and p24 signals present within these individual GFP-Vpr-generated surfaces. This allowed us to selectively analyze the average maximal p24 intensity of fused (S15-mCherry-negative) populations of virions in an unbiased and high-throughput fashion.

First, we observed that unfused (S15-positive) virions exhibited 2.4 times the amount of p24 stain that was observed in fused (S15-negative) virions (Fig. 3C and D; see also Movie S1 in the supplemental material). This demonstrates that this analysis effectively excludes virions that have not productively entered the cytoplasm, since only ca. one-third of the CA present in a virion is

FIG 1 (A to I) Disruption of microtubules delays HIV-1 uncoating as measured by the CsA withdrawal assay. TRIM-Cyp-expressing OMK cells (A through F) or HeLa cells stably expressing HA-conjugated TRIM-Cyp (G through I) were infected with GFP-conjugated VSV-G-pseudotyped (A, B, C, G, H, and I) or A-MLV Env-pseudotyped (D through F) HIV-1 in the presence or absence of 2.5 μM cyclosporine (CsA) with either DMSO or 10 μM nocodazole. Nocodazole was washed out of the cells 2 h after synchronized infection, while CsA was washed out at the time points indicated on the graphs (A, B, D, E, G, and H) or overnight (C, F, and I). For time points earlier than 2 h, CsA-containing medium was removed and replaced with medium containing Noc or DMSO. Forty-eight hours postinfection, cells were analyzed by fluorescence-activated cell sorting for GFP expression. Raw infectivity data representative of 3 or more independent experiments (A, D, and G) and means (± SEM) of results from three independent experiments that were normalized to the results at their respective 4-h time points (B, E, and H) are shown. Statistical significance was calculated by a multiple-comparison *t* test (*, $P < 0.05$; **, $P < 0.01$). (J) The BlaM-Vpr fusion assay was performed in OMK cells and HeLa cells in the presence of DMSO or nocodazole with various inputs of virus (undiluted [Neat] or diluted 1:2, 1:4, or 1:8). Data are means (± SEM) of results from three independent experiments that were normalized to the results for the sample treated with undiluted virus and DMSO. *, $P < 0.05$.

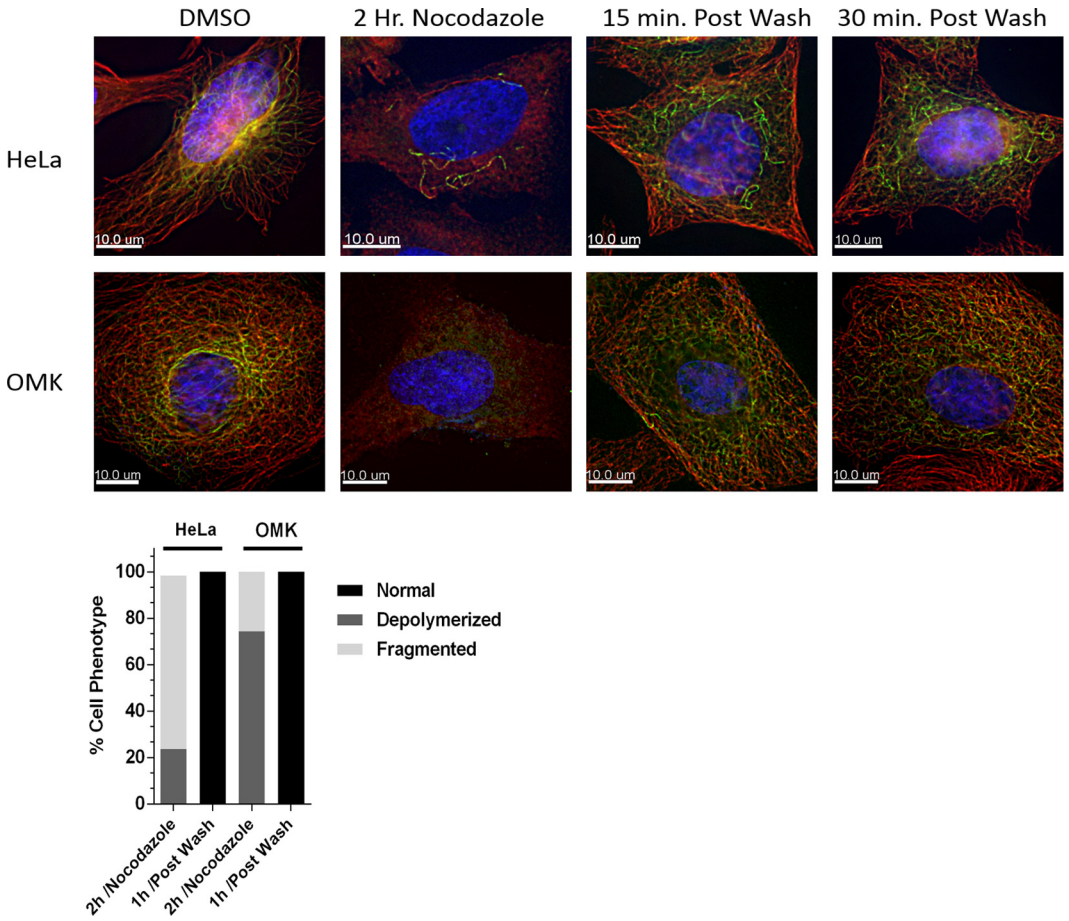

FIG 2 Microtubules re-form rapidly following Noc withdrawal. OMK and HeLa cells were treated with either DMSO or 10 μM nocodazole for 2 h; then nocodazole was removed, and cells were observed after 15 min, 30 min, or 1 h. (Top) Representative images of cells stained for stable (green) and dynamic (red) microtubules. (Bottom) Depolymerized or fragmented (with few microtubules intact) cells were quantified after 2 h of nocodazole treatment or 1 h post-nocodazole removal. Cells in 20 fields were analyzed for each condition.

used to form the mature fullerene capsid core (31, 32), while the remainder is free to diffuse away from the viral particle following fusion.

OMK cells were then infected with GFP-Vpr- and S15-mCherry-labeled virus in the presence or absence of Noc, and CsA was included throughout these experiments to inactivate TRIM-Cyp during these infections. We then plotted the distribution of the intensities of p24 staining of individual GFP-Vpr-positive, S15-mCherry-negative virion populations at various times postinfection. Normalized and averaged data from three independent experiments showed than cytoplasmic virion populations exhibited significantly more p24 staining in the presence of Noc than in its absence (Fig. 4A, dot blot), which was readily apparent when the average maximal p24 intensities were plotted (Fig. 4A, line graph). This effect was apparent 1 h after infection and remained significant throughout the course of the experiment.

We also utilized these data to assess the fusion states of the viral populations in the cells during the experiment. Although we observed by using the Vpr-BlaM assay that fusion was not inhibited in Noc-treated cells (Fig. 1J), this endpoint assay does not address the possibility that Noc treatment could temporarily delay VSV-G-mediated fusion, which could lead to a delay in viral entry in these and previous experiments. To assess this possibility, we determined the percentage of virions at each time point that were S15 positive (unfused) or S15 negative (fused) in order to calculate the relative fusion kinetics occurring during this experiment. Rather than being delayed in Noc-treated cells, which might explain the delay in uncoating, fusion at early time points following infection occurred more rapidly in Noc-treated cells (Fig. 4B). This is generally consistent with the slight increase in the percentage of fusion that was detected using the BlaM-Vpr assay (Fig. 1J). The increase in the level of fusion at early time points in the presence of Noc would be expected to increase the rate at which virions become insensitive to CsA withdrawal, in the absence of an effect of Noc treatment on uncoating. This suggests that the delay in uncoating measured in this assay and the CsA withdrawal assay may actually underrepresent the magnitude of the uncoating defect induced by microtubule disruption, given that both measures of fusion indicate an increase, rather than a delay, in fusion in the presence of Noc. Collectively, these data support the observations made using the CsA withdrawal assay, demonstrating that microtubule disruption with Noc prevents the normal uncoating of the HIV-1 core.

A similar effect was observed after the depolymerization of microtubules with Noc in normal HeLa cells. No CsA was included in these infections, since these cells did not express TRIM-

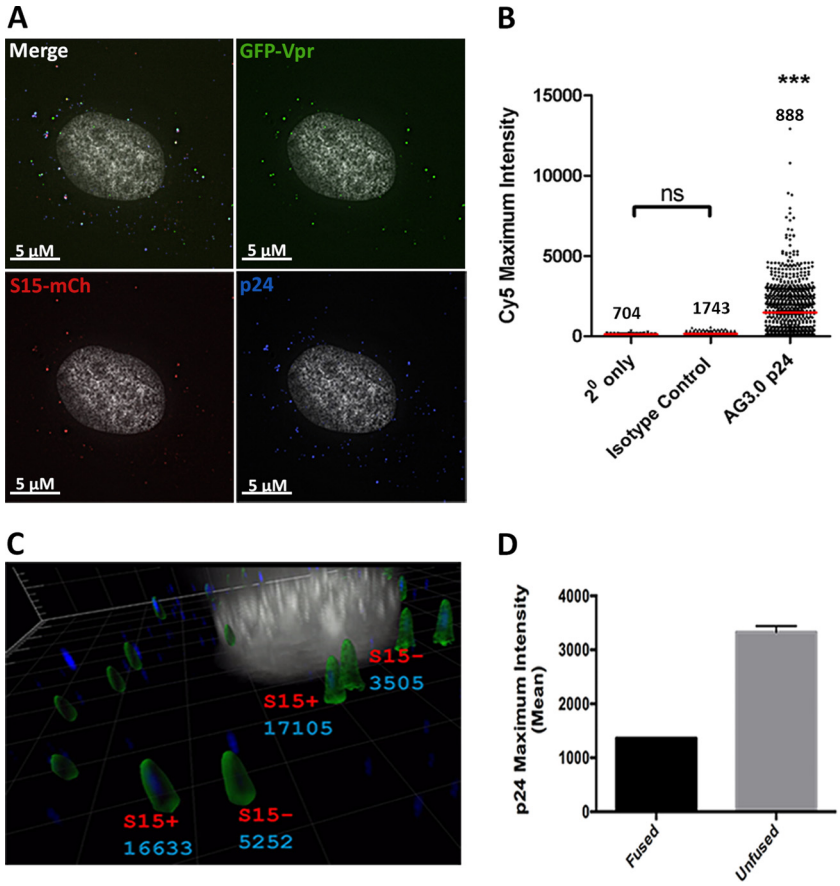

FIG 3 *In situ* assay to measure HIV-1 uncoating. (A) Cells were infected with S15-mCherry- and GFP-Vpr-labeled VSV-G-pseudotyped HIV-1 and were stained for p24 by utilizing antibody AG3.0. Shown is a representative image in different channels obtained during the quantification process. The nuclei of the cells are shown in gray, GFP-Vpr in green, S15-mCherry in red, and p24 staining in blue. (B) Background levels from staining with a Cy5-conjugated secondary antibody were quantified using the secondary antibody only or an isotype control (1 μg/ml). Red lines indicate means. The number of viruses analyzed per condition is given above each data set. ns, not significant; ***, $P < 0.001$. (C) Still image from an animated movie of the image in panel A (see Movie S1 in the supplemental material). (D) Viruses were separated into fused and unfused populations based on the intensity of the S15-mCherry signal within each virus, and the average maximum fluorescence intensities of p24 were plotted. Specific details on the quantification are given in Materials and Methods.

Cyp. A Noc-dependent increase in p24 staining intensity was observed at early times following infection. This difference was significant at all time points examined (Fig. 4C, dot and line graph). Notably, relative to the number in OMK cells, very few GFP-Vpr-positive particles were observed in HeLa cells 4 h following infection (Fig. 4C, dot blot), perhaps affecting our ability to measure an uncoating defect in Noc-treated cells, leading to a reduced degree of statistically significant difference between Noc-treated and control cells at this time point. Cell type-specific differences may account for the differences observed at this time point. Also, no defect in fusion was found in HeLa cells following Noc treatment (Fig. 4D).

Collectively, these results recapitulate the results observed using the CsA washout assay, demonstrating that microtubule disruption impairs HIV-1 uncoating.

Microtubule disruption does not inhibit HIV-1 RT. Previously, it was demonstrated that inhibition of reverse transcription (RT) of HIV-1 delays uncoating, suggesting a relationship between the two processes (7, 33). Therefore, we wanted to determine whether reverse transcription and nuclear import of the viral genome were delayed in the absence of intact microtubules. Following infection, OMK cells were treated with Noc for the first 4 h, and late RT and nuclear import (as measured by 2-LTR circles) relative to those with the control (DMSO treatment) were measured. Noc treatment was performed for 4 h to rule out the possibility that microtubule destabilization may perturb RT in this period. OMK cells were used because they produce a more substantial effect on HIV-1 uncoating in the CsA washout assay than in HeLa cells (Fig. 1) and because they were used in previous studies finding that HIV-1 uncoating is RT dependent (7). Within 2 to 4 h after infection, we observed no difference in the generation of late RT products between Noc-treated and control OMK cells (Fig. 5A). Slight differences were observed at 8 to 10 h following infection, although these differences were not statistically significant (Fig. 5B). Noc treatment had a modest effect on 2-LTR circle formation following an overnight infection (16 h), but again, these differences were not statistically significant (Fig. 5C). Similar results were observed upon Noc treatment for 2 h (data not shown). This demonstrates that Noc treatment does not directly influence RT in these infections, since any differences observed occurred well after the removal of Noc, a finding supported by similar findings for $CD4^+$ T cells by Yoder et al. (26).

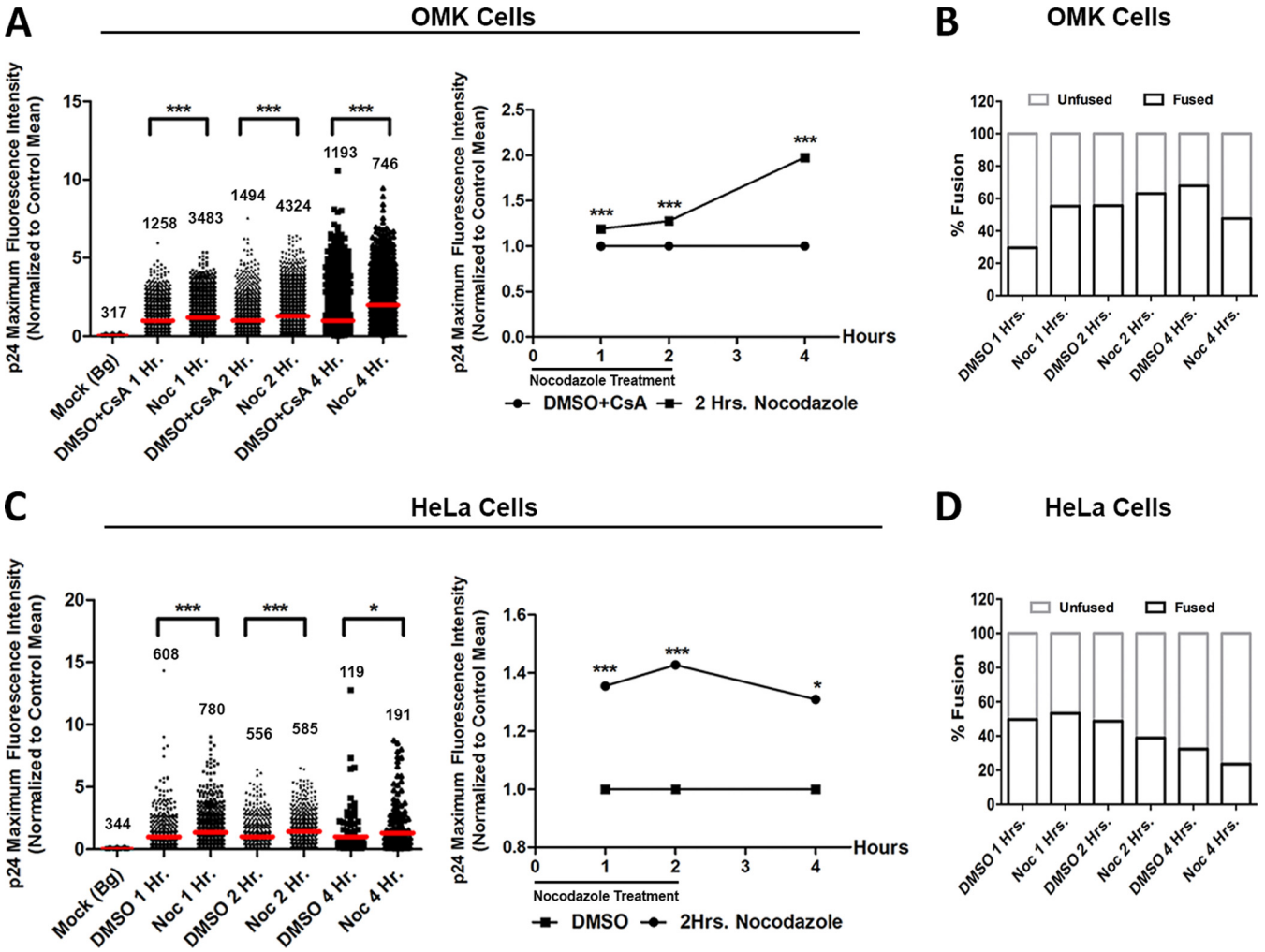

FIG 4 An *in situ* uncoating assay demonstrates an increased level of p24 following microtubule disruption. (A) OMK cells were infected with S15-mCherry- and GFP-Vpr-labeled VSV-G-pseudotyped HIV-1 in the presence of 2.5 μM CsA with either DMSO or 10 μM nocodazole and were fixed at the indicated time points. Viruses were analyzed as described in Materials and Methods. (Left) Each point on the dot blot represents the analysis of an individual virus. Red lines indicate means. The number of viruses analyzed per condition is given above each data set. ***, $P < 0.001$. (Right) The means of the maximum fluorescence intensities of p24 are plotted on the line graph. Data from three independent experiments were normalized and averaged. (B) The percentage of fusion was calculated by determining the percentage of viruses that were S15-mCherry negative (Fused) in the entire population. Statistical significance was determined by one-way ANOVA. (C) Normal HeLa cells were infected with S15-mCherry- and GFP-Vpr-labeled VSV-G-pseudotyped HIV-1 in the presence of DMSO or 10 μM nocodazole and were fixed at the indicated time points. (Left) Analysis was carried out as for panel A. Red lines indicate means. The number of viruses analyzed per condition is given above each data set. Statistical significance was determined by one-way ANOVA (***, $P < 0.001$; *, $P < 0.05$). (Right) The means of the maximum fluorescence intensities of p24 are plotted on the line graph. Data from three independent experiments were normalized and averaged. (D) The percentage of fusion was calculated as described for panel B.

The fate-of-capsid assay confirms microtubule-dependent uncoating of HIV-1. Additionally, the fate-of-capsid assay (22) was utilized to monitor the fate of viral cores in the presence or absence of Noc. As a control, we also included cells expressing rhesus macaque TRIM5α (rhTRIM5α), which is known to induce the premature destabilization of the HIV-1 core in this assay (21). As observed in the other two uncoating assays, Noc treatment enhanced the recovery of intact HIV-1 cores following infection, leading to a 4-fold increase in the amount of intact cores (Fig. 6A). As expected, rhTRIM5α induced the opposite effect, destabilizing HIV-1 cores. Notably, the rhTRIM5α-mediated destabilization of HIV-1 cores was reduced in the presence of Noc, a finding consistent with a previous report (16). However, as demonstrated in the case of TRIM-Cyp restriction, rhTRIM5α restriction of HIV-1 was not abrogated by Noc treatment in HeLa cells stably expressing rhTRIM5α (Fig. 6B). These data provide additional confirmation that microtubule destabilization perturbs the normal uncoating of the HIV-1 core during infection.

Dynein inhibition delays HIV-1 uncoating. The data presented above demonstrate that intact microtubules are required for proper HIV-1 uncoating. However, they reveal nothing about the mechanism by which microtubules facilitate uncoating or the role of microtubule motors during this process. To determine if dynein-mediated trafficking is important for HIV-1 uncoating, we performed the CsA withdrawal assay in the presence of ciliobrevin D (CilioD), a specific inhibitor of dynein-mediated motor function (18). To test the efficacy of this drug, we first asked if CilioD treatment resulted in dispersal of the Golgi apparatus, a

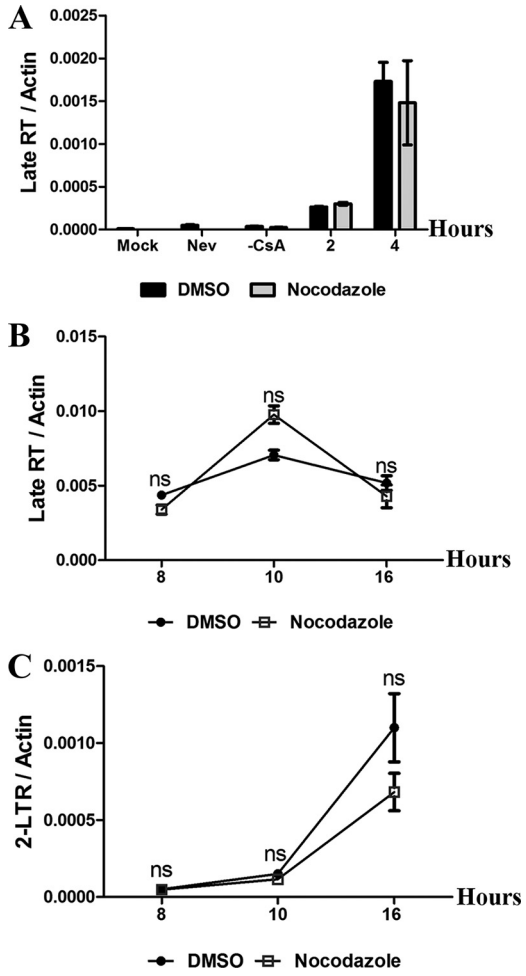

FIG 5 Microtubule destabilization does not affect reverse transcription and nuclear import of HIV-1. OMK cells were infected with GFP-conjugated VSV-G-pseudotyped HIV-1 in the presence of 2.5 μM CsA with either DMSO or 10 μM nocodazole for 4 h following synchronized infection. Following the 4-h treatment, the medium was replaced with fresh medium. Cells were collected at the indicated time points postinfection, and real-time PCR was performed to quantify late RT (A and B) and 2-LTR circles (C). Nevirapine (Nev), an RT inhibitor, was included as a control. ns, not statistically significant.

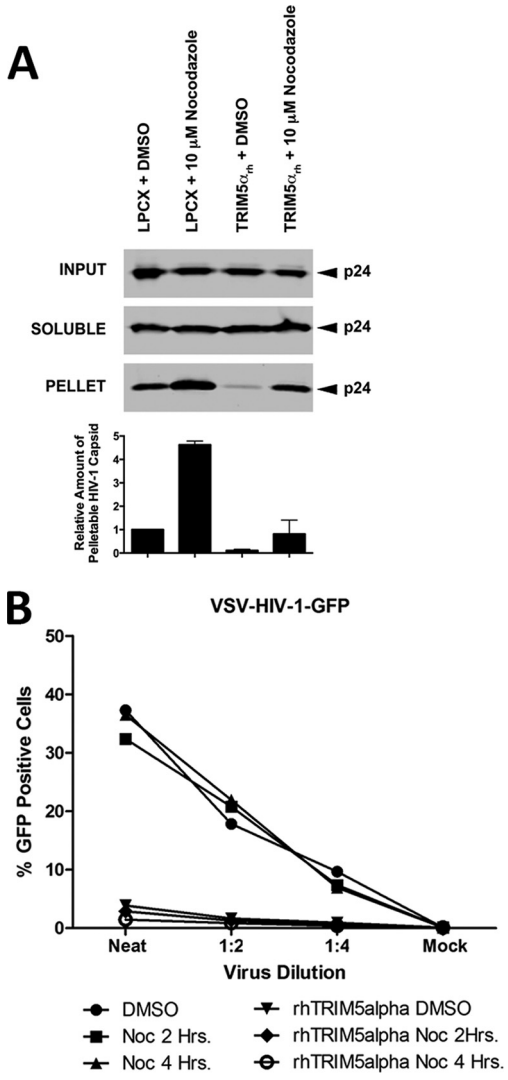

FIG 6 The HIV-1 core is stabilized following microtubule disruption, and rhTRIM5α restriction of HIV-1 is not affected. (A) LPCX-transduced CF2Th cells in the presence of DMSO or 10 μM nocodazole were infected with a GFP reporter virus (VSV-G-pseudotyped HIV-1), and the amounts of soluble capsid and particulate capsid were determined by a fate-of-capsid assay. (B) HeLa cells alone or HeLa cells stably expressing HA-rhTRIM5α were infected with GFP-conjugated VSV-G-pseudotyped HIV-1 in the presence of DMSO or 10 μM nocodazole for 2 or 4 h. Then the medium was replaced with fresh medium, and 48 h postinfection, cells were analyzed by fluorescence-activated cell sorting for GFP expression. Data are means from three independent experiments ± SEM.

well-known consequence of dynein inhibition. As expected, CilioD treatment resulted in the dispersal of the Golgi apparatus in these cells (data not shown). When CilioD was included in the CsA withdrawal assay, we observed a potent and irreversible defect in infectivity (Fig. 7A), in contrast to our observations for brief Noc treatment of OMK and HeLa cells (Fig. 1). While this result is consistent with a dynein-dependent defect in uncoating, the irreversible perturbation of infectivity precludes the conclusion that dynein inhibition directly influences uncoating as determined by the CsA washout assay (Fig. 7A).

We therefore utilized siRNA knockdown of the dynein heavy chain (DYNC1H1) (Fig. 7B) to assess the role of dynein by using our *in situ* uncoating assay. As observed with Noc treatment, DYNC1H1 knockdown led to a significant increase in the amount of p24 associated with GFP-Vpr-positive, S15-mCherry-negative virions (Fig. 7C).A significant defect in uncoating was observed at 1 h postinfection and remained present 4 h following infection (Fig. 7C, dot blot and line graph). As observed in our experiments with Noc, fusion was not significantly affected in cells in which DYNC1H1 was knocked down (Fig. 7D); the slight decrease in fusion observed in DYNC1H1 knockdown cells could be due to a defect in the degradation pathway upon DYNC1H1 knockdown, resulting in an accumulation of more virions in the vesicular compartment in these cells than in control cells. This is supported by the observation of a higher number of unfused virions in these knockdown cells (data not shown). Additionally, live-cell imaging utilizing fluorescently labeled HIV-1 was performed on cells in which DYNC1H1 was knocked down. In these cells, we observed a decrease in the average speed of viruses 30 min after synchronized infection (Fig. 7E), confirming previous data re-

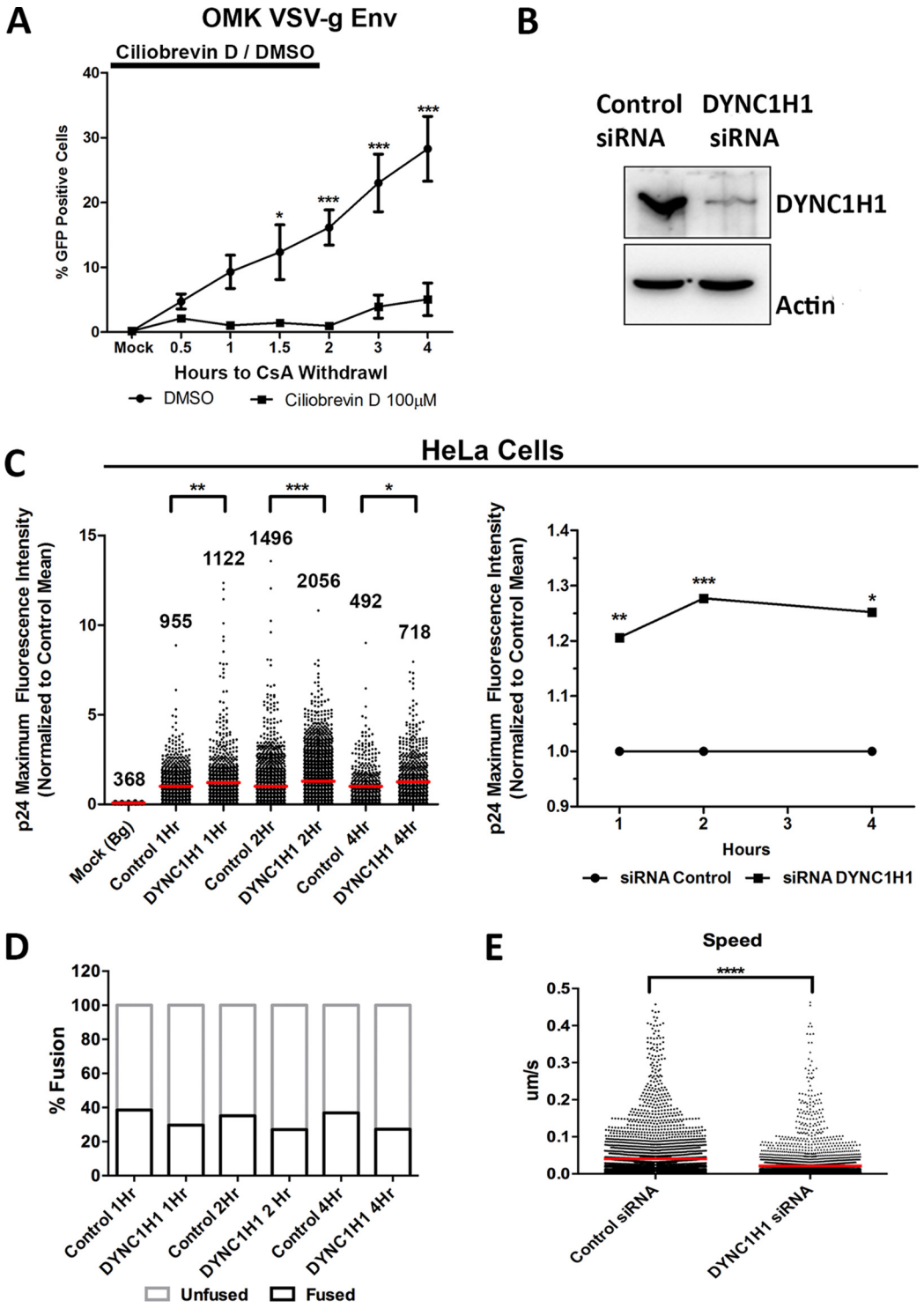

FIG 7 Dynein inhibition delays HIV-1 uncoating. (A) OMK cells were infected with GFP-conjugated VSV-G-pseudotyped HIV-1 in the presence of 2.5 μM CsA with either DMSO or 100 μM ciliobrevin D in medium containing 1% FBS. Ciliobrevin D was washed out of the culture 2 h after synchronized infection, while CsA was washed out at the time points indicated. Forty-eight hours postinfection, cells were analyzed for GFP expression by fluorescence-activated cell sorting. Data are means for three independent experiments ± SEM. Asterisks indicate significant differences (*, $P < 0.05$; ***, $P < 0.001$) by a multiple-comparison *t* test. (B) HeLa cells were treated with control siRNA or siRNA targeting cytoplasmic dynein heavy chain (DYNC1H1) for 72 h. The level of DYNC1H1 was determined by Western blotting with a DYNC1H1-specific antibody. Equal loading was verified with an anti-actin antibody. (C) HeLa cells treated with control or DYNC1H1 siRNA for 72 h were infected with S15-mCherry- and GFP-Vpr-labeled VSV-G-pseudotyped HIV-1 by a synchronized infection. Cells were fixed at the indicated time points postinfection and were stained for p24 in order to perform the *in situ* uncoating assay as described in Materials and Methods. (Left) Each point on the dot blot represents the analysis of an individual virus and is normalized to the mean result for the control at the same time point. Red lines indicate means. The number of viruses analyzed per condition is given above each data set. Statistical significance was determined by one-way ANOVA (***, $P < 0.001$; **, $P < 0.01$; *, $P < 0.05$). (Right) The means of the p24 fluorescence intensities are plotted on the line graph. Data from three independent experiments were normalized and averaged. (D) The percentage of fusion was calculated by determining the percentage of viruses that were S15-mCherry negative (Fused) in the entire population. (E) HeLa cells treated with control siRNA or DYNC1H1 siRNA for 72 h were infected with S15-mCherry- and GFP-Vpr-labeled VSV-G-pseudotyped HIV-1, and live-cell imaging was performed 30 min after a synchronized infection. The speeds of individual viruses were quantified in Imaris software by generating tracks to follow the movement of individual viruses.

ported by McDonald et al. on dynein-dependent HIV-1 trafficking in cells (6). These data reveal that HIV-1 uncoating is facilitated by dynein motor function, since siRNA knockdown of DYNC1H1 increased the amount of p24 associated with cytoplasmic virions, and a corresponding defect in viral trafficking was observed in cells depleted of DYNC1H1.

KIF5B knockdown delays HIV-1 uncoating. Previous studies of HIV-1 trafficking revealed that inhibition of dynein motor function resulted in the accumulation of HIV-1 virions at the cell periphery (6). This suggests that in addition to dynein-mediated trafficking, the viral core can also undergo kinesin-mediated trafficking, although in the absence of perturbation, the cumulative effect of these two transport activities results in minus-end-directed transport toward the MTOC. To test the hypothesis that kinesin motor function can facilitate HIV-1 uncoating, we examined the effect of perturbing kinesin trafficking. The most conventional member of the kinesin family, KIF5B, was chosen, because it has been reported previously to interact with Nup358 to facilitate adenovirus uncoating (34). As was observed with CilioD, KIF5B knockdown (Fig. 8A) resulted in a ~50% reduction in infectivity from that for control siRNA-transfected cells (Fig. 8B).

We therefore used the *in situ* uncoating assay to measure the effect of KIF5B knockdown by siRNA on HIV-1 uncoating. These experiments yielded two somewhat contradictory observations. In three independent experiments, the level of CA staining at 1 h was reduced in KIF5B knockdown cells from that in control cells, a trend that was also apparent when the data from these experiments were pooled (Fig. 8C, dot blot and line graph). However, at later time points, significantly more CA staining was observed in KIF5B knockdown cells than in control siRNA-transfected cells (Fig. 8C, dot blot and line graph). No difference in relative fusion, as measured by S15 membrane labeling, was observed between control and KIF5B siRNA-treated cells (Fig. 8D). These data suggest a role for the plus-end-directed motor KIF5B in HIV-1 uncoating.

DISCUSSION

The data presented above establish that microtubule trafficking facilitates the uncoating of the HIV-1 capsid core during infection. This conclusion is supported by two assay systems commonly utilized to measure uncoating (22, 24) and an *in situ* uncoating assay that we have employed to directly and quantitatively assess the uncoating states of viral populations following synchronized infection.

Previously, investigators examining the role of microtubules have observed superficially divergent results regarding the role of microtubules during HIV-1 infection. McDonald et al. observed that HIV-1 is trafficked to the microtubule-organizing center (MTOC) in a dynein-dependent fashion (6), although that study did not measure the effect of microtubule disruption or dynein inhibition on HIV-1 infection. Sabo et al. recently reported that stable microtubules facilitate early events in infection (13). However, another study observed no effect on infectivity when microtubules were disrupted using Noc (26). The data presented here are consistent with all three studies. Like Yoder et al., we observe that brief microtubule destabilization (2 h) has little or no effect on infectivity in OMK and HeLa cells (26) (Fig. 1C, F, and I). Also in line with the findings of Yoder et al., examination of RT during and after Noc treatment revealed no effect during Noc treatment and only slight but statistically insignificant differences in late-RT and 2-LTR circle levels at later times in infection (Fig. 5). Given the rapid restoration of microtubules observed after Noc withdrawal (Fig. 2), this result is not surprising. These slight changes later in infection may be due to early disruption of uncoating by Noc treatment, although this conclusion cannot be drawn from these experiments. However, we also observe that Noc treatment induces core stabilization that is rapidly reversed following Noc withdrawal (Fig. 1A, B, D, E, G, and H), suggesting that measurement of HIV-1 infectivity following transient Noc treatment may not reveal critical microtubule-dependent aspects of infection, since microtubule-dependent steps in infection may proceed rapidly following Noc withdrawal. This is supported by the observation that cytoplasmic dynein inhibition with CilioD substantially reduces the level of infection (Fig. 7A). Thus, our data collectively support the role of microtubules in HIV-1 trafficking and infection reported by McDonald et al. and Sabo et al. (6, 13), although they are also in general agreement with the results of Yoder et al. (26). Notably, McDonald et al. reported that inhibition of dynein not only prevented the accumulation of viruses at the MTOC but also resulted in the pronounced dispersal of HIV-1 virions to the cell periphery (6), strongly suggesting that the viral core can engage kinesin motors as well as dynein motors. This is consistent with our observation that KIF5B knockdown plays a role in HIV-1 uncoating (Fig. 8C).

Superficially, our observation that Noc treatment does not alter restriction by TRIM-Cyp and rhTRIM5α disagrees with a recent report suggesting that TRIM5α restriction requires intact microtubules (16). However, differences in the period and concentration of Noc treatment, and the viral inoculum used in these infections, could explain these differences. At a minimum, we observe that treatment with Noc for short periods (2 h), the time frame within which TRIM5α and TRIM-Cyp restriction has been reported to occur (8, 14, 35), does not affect restriction by TRIM-Cyp or rhTRIM5α (Fig. 1 and 6). We do, however, observe stabilization of HIV-1 capsids in rhTRIM5α-expressing cells following microtubule destabilization, in agreement with the results of Pawlica et al. (16), supporting a measured approach to consideration of other, more disparate outcomes between these two studies.

The data provided here demonstrate that both dynein heavy chain activity and KIF5B activity facilitate HIV-1 uncoating (Fig. 7 and 8), and a number of mechanisms may explain this observation. Perhaps the simplest model is that the motors engage the viral core and induce its disassembly by providing mechanical force in a so called "tug of war," pulling the capsid cargo in opposite directions along the microtubule. This concept has been proposed in the field of molecular motors (36, 37) and in the trafficking of the HIV-1 core (19), and such observations have been reported previously for the uncoating of herpes simplex virus 1 (HSV-1) (38). Alternatively, it is possible that interaction with motor proteins allows the core to be optimally situated spatiotemporally for uncoating to occur. One obvious scenario of this type would be that dynein transport allows trafficking to the MTOC, where the core engages nuclear pore components that may be involved in uncoating, such as Nup358 (10). Remarkably, an almost identical situation has been described for adenovirus infection, where disassembly of the viral core requires interaction with Nup358 and kinesin 1 (34). In the experiments reported here, the vast majority of virions analyzed in our *in situ* uncoating assay were in the cytoplasm and were not observed to be associated with the nuclear pore by use of a specific monoclonal antibody. However, it is possible that transient but critical uncoating events, which are not detected by use of this assay and fixed images, occur

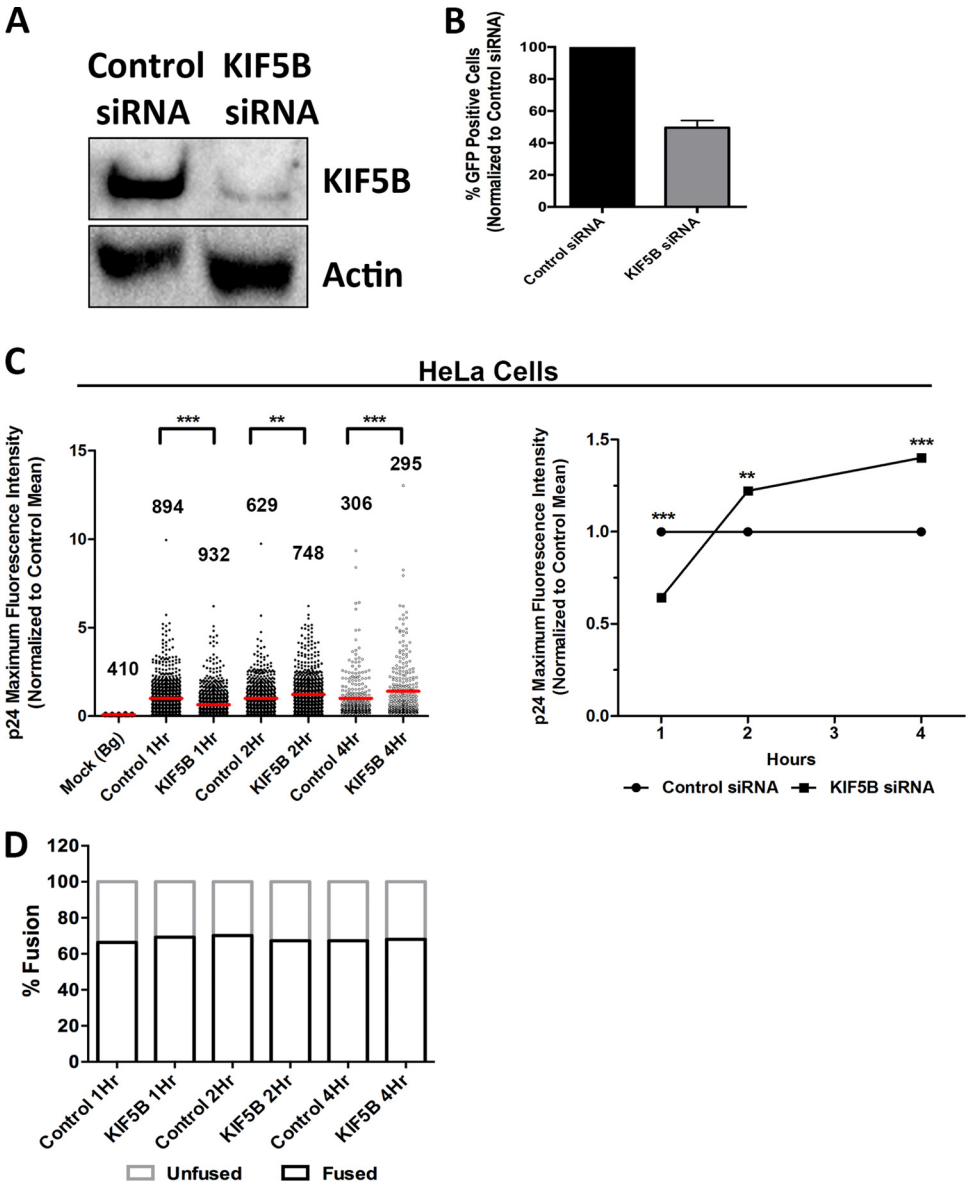

FIG 8 KIF5B knockdown delays HIV-1 uncoating. (A) HeLa cells were treated with control siRNA or siRNA targeting kinesin 1 heavy chain (KIF5B) for 72 h. The level of KIF5B was determined by Western blotting with a kinesin 1 heavy-chain-specific antibody. Equal loading was verified with an anti-actin antibody. (B) HeLa cells treated with control siRNA or KIF5B siRNA were subsequently infected with GFP-conjugated VSV-G-pseudotyped HIV-1. Cells were collected 48 h postinfection and were analyzed by fluorescence-activated cell sorting for GFP positivity. (C) HeLa cells were treated with control siRNA or KIF5B siRNA for 72 h, followed by synchronized infection with S15-mCherry- and GFP-Vpr-labeled VSV-G-pseudotyped HIV-1. Cells were fixed at different time points postinfection and were stained for p24 in order to perform the *in situ* uncoating assay as described in Materials and Methods. (Left) Each point on the dot blot represents the analysis of an individual virus and is normalized to the mean result for the control at the same time point. Red lines indicate means. The number of viruses analyzed per condition is given above each data set. Statistical significance was determined by one-way ANOVA (***, $P < 0.001$; **, $P < 0.01$). (Right) The means of p24 fluorescence intensities are plotted on the line graph. Data from three independent experiments were normalized and averaged. (D) The percentage of fusion was calculated by determining the percentage of viruses that were S15-mCherry negative (Fused) in the entire population.

at the nuclear pore. It is also possible that association with microtubule motors facilitates additional interactions with microtubule-associated proteins (MAPs) such as EB1, critical for early infection, which, in turn, mediate the uncoating event identified in our assays (13).

ACKNOWLEDGMENTS

This work was supported by NIAID grants R01 AI093258 and R21 AI106547 to E.M.C., NIAID grant R01 AI087390 to F.D.-G., and a Schmitt Foundation fellowship to Z.L.

REFERENCES

1. **Coffin JM, Hughes SH, Varmus HE.** 1997. Retroviruses. Cold Spring Harbor Laboratory Press, Cold Spring Harbor, NY.
2. **Butler SL, Hansen MS, Bushman FD.** 2001. A quantitative assay for HIV DNA integration in vivo. Nat. Med. 7:631–634. http://dx.doi.org/10.1038/87979.
3. **Fassati A, Goff SP.** 2001. Characterization of intracellular reverse transcription complexes of human immunodeficiency virus type 1. J. Virol. 75:3626–3635. http://dx.doi.org/10.1128/JVI.75.8.3626-3635.2001.
4. **Fassati A, Goff SP.** 1999. Characterization of intracellular reverse transcription complexes of Moloney murine leukemia virus. J. Virol. 73:8919–8925.

5. **Miller MD, Farnet CM, Bushman FD.** 1997. Human immunodeficiency virus type 1 preintegration complexes: studies of organization and composition. J. Virol. **71:**5382–5390.
6. **McDonald D, Vodicka MA, Lucero G, Svitkina TM, Borisy GG, Emerman M, Hope TJ.** 2002. Visualization of the intracellular behavior of HIV in living cells. J. Cell Biol. **159:**441–452. http://dx.doi.org/10.1083/jcb.200203150.
7. **Hulme AE, Perez O, Hope TJ.** 2011. Complementary assays reveal a relationship between HIV-1 uncoating and reverse transcription. Proc. Natl. Acad. Sci. U. S. A. **108:**9975–9980. http://dx.doi.org/10.1073/pnas.1014522108.
8. **Perez-Caballero D, Hatziioannou T, Zhang F, Cowan S, Bieniasz PD.** 2005. Restriction of human immunodeficiency virus type 1 by TRIM-CypA occurs with rapid kinetics and independently of cytoplasmic bodies, ubiquitin, and proteasome activity. J. Virol. **79:**15567–15572. http://dx.doi.org/10.1128/JVI.79.24.15567-15572.2005.
9. **Lee K, Ambrose Z, Martin TD, Oztop I, Mulky A, Julias JG, Vandegraaff N, Baumann JG, Wang R, Yuen W, Takemura T, Shelton K, Taniuchi I, Li Y, Sodroski J, Littman DR, Coffin JM, Hughes SH, Unutmaz D, Engelman A, KewalRamani VN.** 2010. Flexible use of nuclear import pathways by HIV-1. Cell Host Microbe **7:**221–233. http://dx.doi.org/10.1016/j.chom.2010.02.007.
10. **Schaller T, Ocwieja KE, Rasaiyaah J, Price AJ, Brady TL, Roth SL, Hue S, Fletcher AJ, Lee K, KewalRamani VN, Noursadeghi M, Jenner RG, James LC, Bushman FD, Towers GJ.** 2011. HIV-1 capsid-cyclophilin interactions determine nuclear import pathway, integration targeting and replication efficiency. PLoS Pathog. **7:**e1002439. http://dx.doi.org/10.1371/journal.ppat.1002439.
11. **Yamashita M, Emerman M.** 2004. Capsid is a dominant determinant of retrovirus infectivity in nondividing cells. J. Virol. **78:**5670–5678. http://dx.doi.org/10.1128/JVI.78.11.5670-5678.2004.
12. **Zhou L, Sokolskaja E, Jolly C, James W, Cowley SA, Fassati A.** 2011. Transportin 3 promotes a nuclear maturation step required for efficient HIV-1 integration. PLoS Pathog. **7:**e1002194. http://dx.doi.org/10.1371/journal.ppat.1002194.
13. **Sabo Y, Walsh D, Barry DS, Tinaztepe S, de Los Santos K, Goff SP, Gundersen GG, Naghavi MH.** 2013. HIV-1 induces the formation of stable microtubules to enhance early infection. Cell Host Microbe **14:**535–546. http://dx.doi.org/10.1016/j.chom.2013.10.012.
14. **Campbell EM, Perez O, Anderson JL, Hope TJ.** 2008. Visualization of a proteasome-independent intermediate during restriction of HIV-1 by rhesus TRIM5α. J. Cell Biol. **180:**549–561. http://dx.doi.org/10.1083/jcb.200706154.
15. **Lehmann M, Milev MP, Abrahamyan L, Yao XJ, Pante N, Mouland AJ.** 2009. Intracellular transport of human immunodeficiency virus type 1 genomic RNA and viral production are dependent on dynein motor function and late endosome positioning. J. Biol. Chem. **284:**14572–14585. http://dx.doi.org/10.1074/jbc.M808531200.
16. **Pawlica P, Le Sage V, Poccardi N, Tremblay MJ, Mouland AJ, Berthoux L.** 2014. Functional evidence for the involvement of microtubules and dynein motor complexes in TRIM5α-mediated restriction of retroviruses. J. Virol. **88:**5661–5676. http://dx.doi.org/10.1128/JVI.03717-13.
17. **Gupta V, Palmer KJ, Spence P, Hudson A, Stephens DJ.** 2008. Kinesin-1 (uKHC/KIF5B) is required for bidirectional motility of ER exit sites and efficient ER-to-Golgi transport. Traffic **9:**1850–1866. http://dx.doi.org/10.1111/j.1600-0854.2008.00811.x.
18. **Firestone AJ, Weinger JS, Maldonado M, Barlan K, Langston LD, O'Donnell M, Gelfand VI, Kapoor TM, Chen JK.** 2012. Small-molecule inhibitors of the AAA+ ATPase motor cytoplasmic dynein. Nature **484:**125–129. http://dx.doi.org/10.1038/nature10936.
19. **Gaudin R, de Alencar BC, Arhel N, Benaroch P.** 2013. HIV trafficking in host cells: motors wanted! Trends Cell Biol. **23:**652–662. http://dx.doi.org/10.1016/j.tcb.2013.09.004.
20. **Simm M, Shahabuddin M, Chao W, Allan JS, Volsky DJ.** 1995. Aberrant Gag protein composition of a human immunodeficiency virus type 1 *vif* mutant produced in primary lymphocytes. J. Virol. **69:**4582–4586.
21. **Stremlau M, Perron M, Lee M, Li Y, Song B, Javanbakht H, Diaz-Griffero F, Anderson DJ, Sundquist WI, Sodroski J.** 2006. Specific recognition and accelerated uncoating of retroviral capsids by the TRIM5α restriction factor. Proc. Natl. Acad. Sci. U. S. A. **103:**5514–5519. http://dx.doi.org/10.1073/pnas.0509996103.
22. **Yang Y, Luban J, Diaz-Griffero F.** 2014. The fate of HIV-1 capsid: a biochemical assay for HIV-1 uncoating. Methods Mol. Biol. **1087:**29–36. http://dx.doi.org/10.1007/978-1-62703-670-2_3.
23. **Wu X, Anderson JL, Campbell EM, Joseph AM, Hope TJ.** 2006. Proteasome inhibitors uncouple rhesus TRIM5α restriction of HIV-1 reverse transcription and infection. Proc. Natl. Acad. Sci. U. S. A. **103:**7465–7470. http://dx.doi.org/10.1073/pnas.0510483103.
24. **Hulme AE, Hope TJ.** 2014. The cyclosporin A washout assay to detect HIV-1 uncoating in infected cells. Methods Mol. Biol. **1087:**37–46. http://dx.doi.org/10.1007/978-1-62703-670-2_4.
25. **Sayah DM, Sokolskaja E, Berthoux L, Luban J.** 2004. Cyclophilin A retrotransposition into TRIM5 explains owl monkey resistance to HIV-1. Nature **430:**569–573. http://dx.doi.org/10.1038/nature02777.
26. **Yoder A, Guo J, Yu D, Cui Z, Zhang XE, Wu Y.** 2011. Effects of microtubule modulators on HIV-1 infection of transformed and resting CD4 T cells. J. Virol. **85:**3020–3024. http://dx.doi.org/10.1128/JVI.02462-10.
27. **Cavrois M, De Noronha C, Greene WC.** 2002. A sensitive and specific enzyme-based assay detecting HIV-1 virion fusion in primary T lymphocytes. Nat. Biotechnol. **20:**1151–1154. http://dx.doi.org/10.1038/nbt745.
28. **Campbell EM, Perez O, Melar M, Hope TJ.** 2007. Labeling HIV-1 virions with two fluorescent proteins allows identification of virions that have productively entered the target cell. Virology **360:**286–293. http://dx.doi.org/10.1016/j.virol.2006.10.025.
29. **Murray JM, Appleton PL, Swedlow JR, Waters JC.** 2007. Evaluating performance in three-dimensional fluorescence microscopy. J. Microsc. **228:**390–405. http://dx.doi.org/10.1111/j.1365-2818.2007.01861.x.
30. **Yuste R (ed).** 2011. Imaging: a laboratory manual, 1st ed, vol 1. Cold Spring Harbor Laboratory Press, Cold Spring Harbor, NY.
31. **Briggs JA, Simon MN, Gross I, Krausslich HG, Fuller SD, Vogt VM, Johnson MC.** 2004. The stoichiometry of Gag protein in HIV-1. Nat. Struct. Mol. Biol. **11:**672–675. http://dx.doi.org/10.1038/nsmb785.
32. **Li S, Hill CP, Sundquist WI, Finch JT.** 2000. Image reconstructions of helical assemblies of the HIV-1 CA protein. Nature **407:**409–413. http://dx.doi.org/10.1038/35030177.
33. **Yang Y, Fricke T, Diaz-Griffero F.** 2013. Inhibition of reverse transcriptase activity increases stability of the HIV-1 core. J. Virol. **87:**683–687. http://dx.doi.org/10.1128/JVI.01228-12.
34. **Strunze S, Engelke MF, Wang IH, Puntener D, Boucke K, Schleich S, Way M, Schoenenberger P, Burckhardt CJ, Greber UF.** 2011. Kinesin-1-mediated capsid disassembly and disruption of the nuclear pore complex promote virus infection. Cell Host Microbe **10:**210–223. http://dx.doi.org/10.1016/j.chom.2011.08.010.
35. **Stremlau M, Owens CM, Perron MJ, Kiessling M, Autissier P, Sodroski J.** 2004. The cytoplasmic body component TRIM5α restricts HIV-1 infection in Old World monkeys. Nature **427:**848–853. http://dx.doi.org/10.1038/nature02343.
36. **Jolly AL, Gelfand VI.** 2011. Bidirectional intracellular transport: utility and mechanism. Biochem. Soc. Trans. **39:**1126–1130. http://dx.doi.org/10.1042/BST0391126.
37. **Welte MA.** 2010. Bidirectional transport: matchmaking for motors. Curr. Biol. **20:**R410–R413. http://dx.doi.org/10.1016/j.cub.2010.03.018.
38. **Radtke K, Kieneke D, Wolfstein A, Michael K, Steffen W, Scholz T, Karger A, Sodeik B.** 2010. Plus- and minus-end directed microtubule motors bind simultaneously to herpes simplex virus capsids using different inner tegument structures. PLoS Pathog. **6:**e1000991. http://dx.doi.org/10.1371/journal.ppat.1000991.